JOURNAL OF OPTOELECTRONICS AND ADVANCED MATERIALS Vol. 16, No. 3 - 4, March – April 2014, p. 276 - 282

Influence of noise mechanism on zero-bias resistance junction-area product in $In_{0.53}Ga_{0.47}As$ photovoltaic infrared detector

YINGTIAN XU[a], YING LI[b], BEIHONG LONG[c], YAN MA[a], GUOTONG DU[a], JINGZHI YIN[a,*]
[a]*State Key Laboratory on Integrated Optoelectronics, College of Electronic Science and Engineering, Jilin University, 2699 Qianjin Street, Changchun, 130012, People's Republic of China*
[b]*Changchun Automobile Industry institute, 9999 Dongfeng street, Changchun, 130011, People's Republic of China*
[c]*College of Materials Science and Engineering, Jinlin University, 2699 Qianjin Street, Changchun, 130012, People's Republic of China*

We theoretically analyze the effects of material parameters on the R_0A product of $In_{0.53}Ga_{0.47}As$ photovoltaic infrared detector by considering the four dominant noise mechanisms. The results show that R_0A is mainly affected by generation-recombination mechanism at the carrier concentration<10^{15}cm^{-3} for the triangular and parabolic potential barriers. Moreover, the effects of surface recombination velocity, its carrier concentration and thickness on R_0A product have also been discussed. The influence of *p*-region material parameters on the R_0A product is larger than that of the *n*-region. $R_0A>10^6(\Omega\bullet cm^2)$ at $p=10^{17}cm^{-3}$, R_0A product of $10^8\Omega\bullet cm^2$ (T=250K) and $10^6\Omega\bullet cm^2$ (T=300K) are obtained.

(Received November 26, 2012; accepted March 13, 2014)

Keywords: A. $In_{0.53}Ga_{0.47}As$ PV detector, D. Noise mechanism, D. Zero-bias resistance junction-area product (R_0A)

1. Introduction

Modern high-performance infrared photovoltaic detector technology, based on photon absorption in narrow-gap semiconductors, has attracted much attention in near infrared applications, such as remote sensing and spectroscope analysis, infrared imaging, optical communication and many other fields. Indium Gallium Arsenide ($In_{1-x}Ga_xAs$) ternary alloys have become important materials for the fabrication of infrared detectors, due to their prominent features such as relatively low dark current density, quick response, as well as high sensitivity and detectivity. The energy gap of the $In_{1-x}Ga_xAs$ ternary system spans from 0.35 *eV* (3.5μm) for *InAs* to 1.43 *eV* (0.87μm) for *GaAs*. $In_{0.53}Ga_{0.47}As$ alloy (E_g=0.73 *eV*, λ_c=1.7μm) lattice matched to the *InP* substrate has already been proved to be a suitable detector material for near-infrared (1.0~1.7μm) spectral range [1-4].

Dark current passing across detector will generate noise because of the statistical nature of the generation and recombination process. Mainly four-type noise mechanisms of infrared detector have been considered, including generation-recombination noise, radiative noise, Auger recombination noise and tunneling noise. Detectivity (denoted as *D**) is an important parameter to measure detector performance, while the noise has great effect on *D**. Therefore, it is indispensable to suppress all kinds of noise mechanisms in order to improve the *D**. In this paper, we theoretically analyze the dependence of the zero-bias resistance junction-area product (R_0A) on material parameters [5-8].

2. Theoretical analysis

The calculation is based on a structure of photodetector, which can be simplified as a *p-n* type of $In_{1-x}Ga_xAs$ deposited on *InP* substrate. The geometry of the photodetector is taken in Fig. 1. Usually, the performance of infrared photovoltaic detector is characterized by the detectivity *D**, which depends on the zero-bias resistance junction-area product (R_0A) and quantum efficiency (η) under negligible background radiation,

$$D^* = \frac{\lambda\eta q}{hc}\sqrt{\frac{R_0A}{4kT}} \tag{1}$$

where η and k are quantum efficiency and Boltzmann constant, respectively. λ is the wavelength of the incidence light, T is the work temperature, c is the velocity of light and q is the charge of an electron.

All the noise mechanisms are independent. When four type noise mechanisms are considered, $(R_0A)_{Total}$ can be expressed by [9]:

$$\frac{1}{(R_0A)_{Total}}=\frac{1}{(R_0A)_{Auger}}+\frac{1}{(R_0A)_{GR}}+\frac{1}{(R_0A)_{Rad}}+\frac{1}{(R_0A)_{Tunnel}} \tag{2}$$

Where $(R_0A)_{Auger}$, $(R_0A)_{GR}$, $(R_0A)_{Rad}$ and $(R_0A)_{Tunnel}$ are determined by Auger recombination noise, generation-recombination noise, radiative noise and tunneling noise.

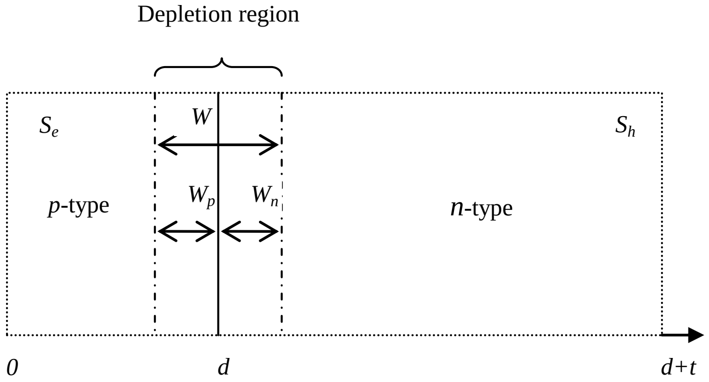

Fig. 1. Schematic 2D structure of $In_{1-x}Ga_xAs$ p-n junction. W is width of depletion region; W_n is width of depletion region on n side; W_p is width of depletion region on p side; t and d are n-region thickness and p-region thickness; S_h and S_e are surface recombination velocity for holes in n region and for electrons in p region; n and p are carrier concentration in n-region and p-region.

2.1 Auger recombination mechanism and Radiative mechanism

Auger recombination mechanism and radiative mechanism are mainly depended on the processes of generation-recombination during the diffusion of minority carriers. Therefore, for Auger recombination mechanism and radiative mechanism, the equations of diffusion current and R_0A are identical with each other. However, the lifetime of minority carriers in *p-n* junction is different.

There are 10 ways about the Auger recombination mechanism. Among them, CCCH, CHHL and CHHS are three fundamental ones. The lifetime of CCCH, CHHL and CHHS in *p*-region and *n*-region can be indicated by [10]:

n-region:
$$\tau^h_{CCCH}=\frac{2\tau^i_{CCCH}}{1+n^2/n_i^2} \tag{3}$$

$$\tau^h_{CHHL}=\frac{2\tau^i_{CHHL}}{1+n_i^2/n^2} \tag{4}$$

$$\tau^h_{CHHS}=\frac{2\tau^i_{CHHS}}{1+n_i^2/n^2} \tag{5}$$

p-region:
$$\tau^e_{CCCH}=\frac{2\tau^i_{CCCH}}{1+n_i^2/p^2} \tag{6}$$

$$\tau^e_{CHHL}=\frac{2\tau^i_{CHHL}}{1+p^2/n_i^2} \tag{7}$$

$$\tau^e_{CHHS}=\frac{2\tau^i_{CHHL}}{1+p^2/n_i^2} \tag{8}$$

n_i and τ^i indicate intrinsic carrier concentration and recombination time.

The radiative lifetime of minority carriers is given by:

(*n*-region)
$$\tau^h_{Rad}=\frac{1}{B(n+n_i^2/n)} \tag{9}$$

(*p*-region)
$$\tau^e_{Rad}=\frac{1}{B(p+n_i^2/p)} \tag{10}$$

B is defined as:

$$B=5.8\times10^{-13}\varepsilon_\infty^{1/2}(\frac{1}{m_e^*+m_h^*})^{3/2}(1+\frac{1}{m_e^*}+\frac{1}{m_h^*})(300/T)^{3/2}Eg^2 \tag{11}$$

Therefore, diffusion current for both Auger recombination mechanism and radiative mechanism can be obtained as [11]:

$$J^h_{Diff}=\frac{qn_i^2}{N_D}\frac{D_h}{L_h}\frac{\gamma_h ch\frac{(t-W_n)}{L_h}+sh\frac{(t-W_n)}{L_h}}{\gamma_h sh\frac{(t-W_n)}{L_h}+ch\frac{(t-W_n)}{L_h}}(e^{\frac{qV}{kT}}-1)$$

(n-region) (12)

$$J^{e}_{Diff} = \frac{qn_i^2}{N_A}\frac{D_e}{L_e}\frac{\gamma_e ch\frac{(d-W_p)}{Le} + sh\frac{(d-W_p)}{L_e}}{\gamma_e sh\frac{(d-W_p)}{L_e} + ch\frac{(d-W_p)}{L_e}}(e^{\frac{qV}{kT}}-1)$$

(p-region) (13)

where $D_i=kT\mu_i/q$, $Li=(D_i\tau_i)^{1/2}$ and $\gamma_i=L_iS_i/D_i$, the angle mark i namely represents e or h. L, S, μ, D and τ are the diffusion length (cm), surface recombination velocity (ms^{-1}), effective mobility ($cm^2V^{-1}s^{-1}$), diffusion coefficient (cm^2s^{-1}), and carrier lifetime (s) for holes in the n region or for electrons in the p region, respectively. n_i is the intrinsic carrier concentration (cm^{-3}). N_D and N_A are donor and acceptor concentrations in p and n regions, respectively.

Due to R_0A product can be expressed as

$$\frac{1}{R} = \frac{dI}{dV}\Big|_{V=0} = A\ \frac{dJ}{dV}\Big|_{V=0} \tag{14}$$

A is device sectional area. The R_0A product in the n and p regions is given respectively by

$$(R_0A)^{h}_{Diff} = \frac{kT}{q^2}\frac{L_hn}{D_hn_i^{\ 2}}\frac{\gamma_h sh(\frac{t-W_n}{L_h}) + ch(\frac{t-W_n}{L_h})}{\gamma_h ch(\frac{t-W_n}{L_h}) + sh(\frac{t-W_n}{L_h})}$$

(n-region) (15)

$$(R_0A)^{e}_{Diff} = \frac{kT}{q^2}\frac{L_ep}{D_en_i^{\ 2}}\frac{\gamma_e sh(\frac{d-W_p}{L_e}) + ch(\frac{d-W_p}{L_e})}{\gamma_e ch(\frac{d-W_p}{L_e}) + sh(\frac{d-W_p}{L_e})}$$

(p-region) (16)

The diffusion current contributions from the n and p regions are added to give the total diffusion current, and the total R_0A product from both sides is

$$\frac{1}{(R_0A)^{Total}_{Diff}} = \frac{1}{(R_0A)^{e}_{Diff}} + \frac{1}{(R_0A)^{h}_{Diff}} \tag{17}$$

2.2 Generation-recombination mechanism

In depletion region, defects and impurities are regarded as intermediate states for the thermal generation and recombination of carriers. These G-R centers are referred as Shockley Read Hall (SRH) centers. The current caused by generation-recombination mechanism can be approximated as [9]:

$$J_{GR} = \frac{2KTn_iWsh(qV/2kT)}{\tau_{SRH}(V_{bi}-V)} \tag{18}$$

W is the depletion region width which is dependent on the voltage. V_{bi} is built-in potential, $\tau_{SRH} = 1/v_{th}\sigma N_f$ is generation-recombination lifetime of SRH. v_{th} is the thermal carrier velocity, σ is the capture cross-section, N_f is the SRH trap density.

The associated $(R_0A)_{GR}$ derivatives as:

$$(R_0A)_{GR} = \frac{V_{bi}}{qn_iWv_{th}\sigma N_f} \tag{19}$$

2.3 Tunneling mechanism

There are two kinds of tunneling current cross the p-n junction, namely, indirect and direct tunneling current. Because the probability for direct tunneling is much larger than that of indirect tunneling, thus only direct tunneling has been considered in this paper. The tunneling current is given by [12, 13]:

$$J_{Tunnel} = \frac{qm^*}{8\pi^2\hbar^3}T_t\frac{qV}{kT}(\delta_n+\delta_p-qV)^2 \tag{20}$$

δ_n and δ_p are the distance between Fermi levels and each side of the junction; T_t is tunneling probability, which is determined by potential barrier shape. For triangular and parabolic barriers, tunneling probability can be expressed as:

$$T_{t1} = \exp(-\frac{4\sqrt{2m^*}Eg^{3/2}W}{3q\hbar V_{bi}})$$

(Triangular barriers) (21)

$$T_{t2} = \exp(-\frac{\pi\sqrt{m^*}Eg^{3/2}W}{2\sqrt{2}q\hbar V_{bi}})$$

(Parabolic barriers) (22)

Therefore, R_0A product is derived from above equations.

$$(R_0A)_{Tunnel} = \frac{8\pi^2\hbar^3kT}{q^2m^*T_t(\delta_n+\delta_p)^2} \tag{23}$$

Material parameters of $In_{1-x}Ga_xAs$ ternary-alloy calculated are obtained by method of linear interpolation. The related material parameters are listed in Table 1.

Table 1. Material parameters used in the calculation [14].

	InAs	*GaAs*
Eg(T)(eV)	$0.420-2.5010^{-4}T^2/(T+75)$	$1.519-5.4010^{-4}T^2/(T+204)$
ε_r	14.5	13.18
m_e^*/m_0	0.023	0.067
m_h^*/m_0	0.41	0.45
m_s^*/m_0	0.089	0.15
Δ	0.38	0.34

3. Results and analysis

Four kinds of noise mechanisms have been effected by material parameters of photovoltaic detectors. We analyzed the influences of carrier concentrations, thickness and surface recombination velocities in the two quasi-neutral regions on R_0A product. The calculation is performed on a *p-n* type of $In_{0.53}Ga_{0.47}As$ deposited on *InP* substrate. *D** (Detectivity), a figure of merit of photodetecters, is limited by zero bias resistance-area product (R_0A), when assuming quantum efficiency $\eta = 1$. In calculation, mobility for the electron and hole are $\mu_e=5000 cm^2/V{\bullet}s$ and $\mu_p=400 cm^2/V{\bullet}s$, respectively.

Fig. 2 shows the variations of the theoretically estimated components of R_0A product (Auger, GR, Rad and Tunnel) and $(R_0A)_{Total}$ with the doping concentration. Fig. 2 (a) and Fig. 2 (b) correspond to the triangular and parabolic potential barriers, respectively. It exactly shows that tunneling mechanism appears in $p>10^{18} cm^{-3}$. This attributes to one necessary requirement for directly tunneling current that both *p*-region and *n*-region must be degenerate. $(R_0A)_{Tunnel}$ sharply drops with increasing the *p*-region carrier concentration. Fig. 2 presents that $(R_0A)_{Total}$ is mainly effected by R_0A product components in three different ranges, located at low doping concentration range ($p<10^{15} cm^{-3}$), high doping concentration range ($p>10^{18} cm^{-3}$) and $10^{15} cm^{-3}<p<10^{18} cm^{-3}$, respectively. Comparing the Fig. 2 (a) with Fig. 2 (b), $(R_0A)_{GR}$ mainly contributes to $(R_0A)_{Total}$ in $p<10^{15} cm^{-3}$, and then tends to saturate at very high doping concentration ($p>10^{19} cm^{-3}$). Furthermore, all the R_0A product components except for the tunneling mechanism have impacted on $(R_0A)_{Total}$ when $10^{15} cm^{-3}<p<10^{18} cm^{-3}$. This is because that the width of the depletion region is comparatively large causing the diffusion and generation-recombination component of current. In this doping range, R_0A component due to tunneling has a much higher value as compared to the other components (Auger, Rad and GR). However, $(R_0A)_{Total}$ is limited by the Auger mechanism on the triangular barrier (a) and by the tunneling mechanism on the parabolic barrier (b) in high *p*-region concentration ($p>10^{18} cm^{-3}$). For parabolic barrier, the tunneling component of R_0A falls below the GR component. At even higher doping concentration, the tunneling component of the R_0A product also falls below the Auger and Rad component. At higher doping levels of the active region, the width of the depletion region decreases significantly and the tunneling component of current starts to dominate over other components. In order to achieve a high value of R_0A product, it is therefore necessary to maintain a low doping concentration in the active region. $(R_0A)_{Total}$ reaches about $10^6 (\Omega{\bullet}cm^2)$ when p is about $10^{17} cm^{-3}$, which is consistent with experimental values reported by Antoni Rogalski et al [15].

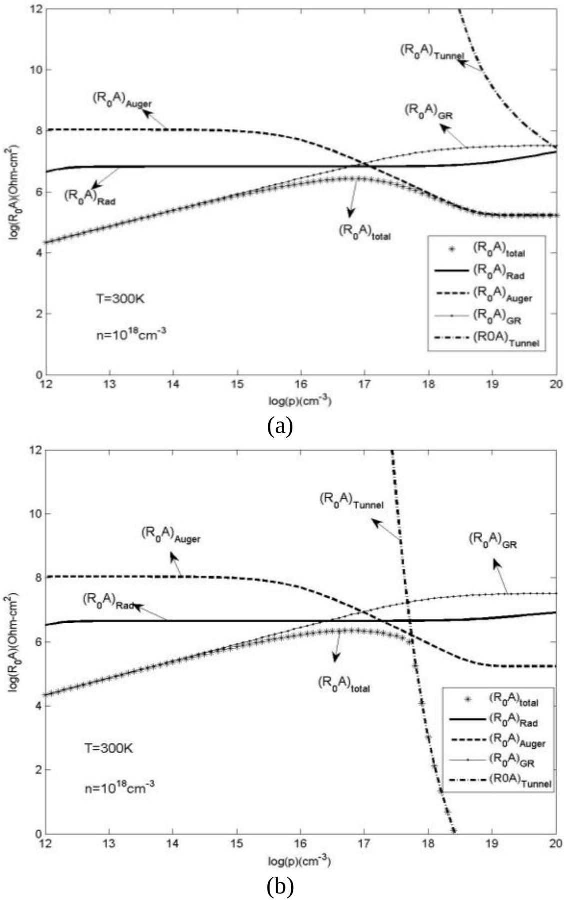

(a)

(b)

Fig. 2. $(R_0A)_{Total}$ and R_0A product components: $(R_0A)_{Auger}$, $(R_0A)_{GR}$, $(R_0A)_{Rad}$ and $(R_0A)_{Tunnel}$ versus the p-region carrier concentration (a) for triangular potential barriers and (b) for parabolic potential barriers. $t=5\mu m$, $d=5\mu m$, $S_e=0$, $S_h=0$.

Fig. 3 compares the ultimate R_0A product of *p*-on-*n* *InGaAs* photodetector with attainable experimental data [16] for wavelength from 1.2*μm* to 2.6*μm*. *InGaAs* photodetector shows high device performance close to theoretical limits for material whose composition is nearly matched to that of *InP* ($\lambda_c \approx 1.7\mu m$). However, their performance decreases rapidly at long wavelengths due to mismatch induced defects with the substrate.

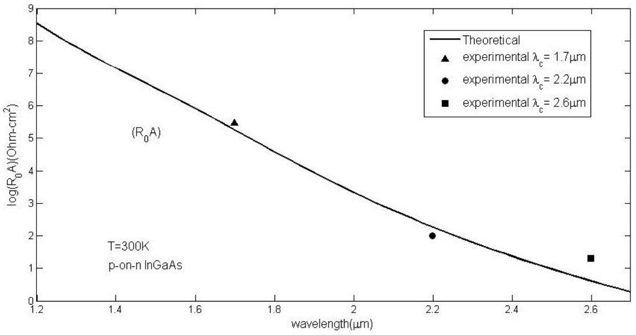

Fig. 3. The dependence of $(R_0A)_{Total}$ product on the wavelength cutoff for p-on-n InGaAs photodetectors at 300K. The experimental values are taken from Ref 16.

The effect of *p*-region carrier concentration on R_0A product with different *p*-side surface recombination velocity (S_e) and thickness (*d*) is shown in Fig. 4. It can be seen from Fig. 4 (a) that R_0A product decreases with increasing S_e at range of $10^{15}cm^{-3}<p<10^{19}cm^{-3}$, while the R_0A product remains almost constant up to a doping concentration of $10^{19}cm^{-3}$. In addition, R_0A product has been found to increase with *p*-region carrier concentration, then appear a peak for $S_e<10^8$ (*m/s*). The largest R_0A product can be obtained about $R_0A>10^6(\Omega\bullet cm^2)$ at $p=10^{17}cm^{-3}$ when the surface recombination velocity for electrons is assumed to be zero and the peak value is about $R_0A>10^5(\Omega\bullet cm^2)$ for $S_e=100$ (*m/s*) and $S_e=10^4$ (*m/s*). Reducing surface recombination velocity is benefit to increasing R_0A product. Therefore, to improve the performance of the detector, surface passivation processes are essential during device fabrication. Fig. 4 (b) depicts the variations of R_0A product with the *p*-region concentration as functions of *p*-region thickness. It distinctly expresses that *p*-region thickness has no effect on R_0A product at low range carrier concentration ($p<10^{15}cm^{-3}$), and R_0A product has been decreased with increasing *d* when $10^{15}cm^{-3}<p<10^{19}cm^{-3}$. Furthermore, the R_0A product of the device increases steadily with increase in doping concentration and reaches a peak value for different *d* and then finally decreases rather fast with a further increase in doping concentration. The largest value of R_0A product has been received about $1og(R_0A)>6.5$ for $d=0.5\mu m$.

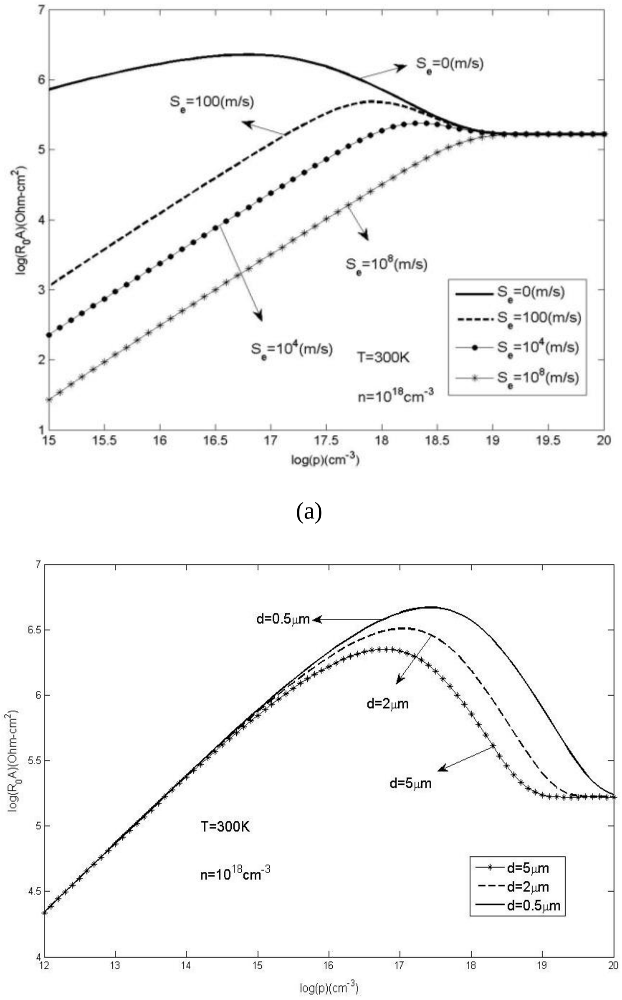

(a)

(b)

Fig. 4. The effect of p-region carrier concentration on R_0A product with different (a) p-side surface recombination velocity and (b) thickness. $t=5\mu m$, $d=5\mu m$, $S_h=0$.

Fig. 5 shows the dependence of R_0A product on *n*-region material parameters. The relationship between R_0A product and *n*-region carrier concentrations with different *n*-side surface recombination velocity (S_h) at $T=250K$ has been expressed in Fig. 5 (a), and R_0A product versus the *n*-region carrier concentrations with diverse thickness (*t*) at $T=300K$ is showed in Fig. 5 (b). The effect of *n*-region parameters on R_0A product is smaller than the *p*-region parameters. Fig. 5 (a) explicitly expresses that R_0A product drops with increasing S_h, but decreasing value from $S_h=0$(*m/s*) to $S_h=10$(*m/s*) is larger than one from $S_h=10$(*m/s*) to $S_h=100$(*m/s*). R_0A product is nearly constant at large surface recombination velocity ($S_h \geq 10m/s$). Furthermore, increasing *n*-region carrier concentrations makes R_0A product augment, and R_0A product can be obtained above $10^8(\Omega\bullet cm^2)$ in $n>10^{16}cm^{-3}$. When $n=10^{18}cm^{-3}$, no matter what values of S_h has been taken, the value of R_0A product keeps constant. Fig. 5 (b) depicts that the trend for R_0A product at different thickness of *n*-region is similar. At the range of $10^{12}cm^{-3}<n<10^{15}cm^{-3}$, varied *t* has no influence on R_0A product. However, R_0A product appears slightly drop with increasing *t* within $10^{15}cm^{-3}<n<10^{18}cm^{-3}$. Moreover, R_0A product increases with increasing *n*, and R_0A product achieves above $10^6(\Omega{\bullet}cm^2)$ in $n>10^{16}cm^{-3}$. As already mentioned, the R_0A product of the device is strongly influenced by the operating temperature. The value of R_0A product is $10^8(\Omega{\bullet}cm^2)$ at T=250K and $10^6(\Omega{\bullet}cm^2)$ at T=300K, respectively, which has been confirmed in the literature of A. Rogalski [17].

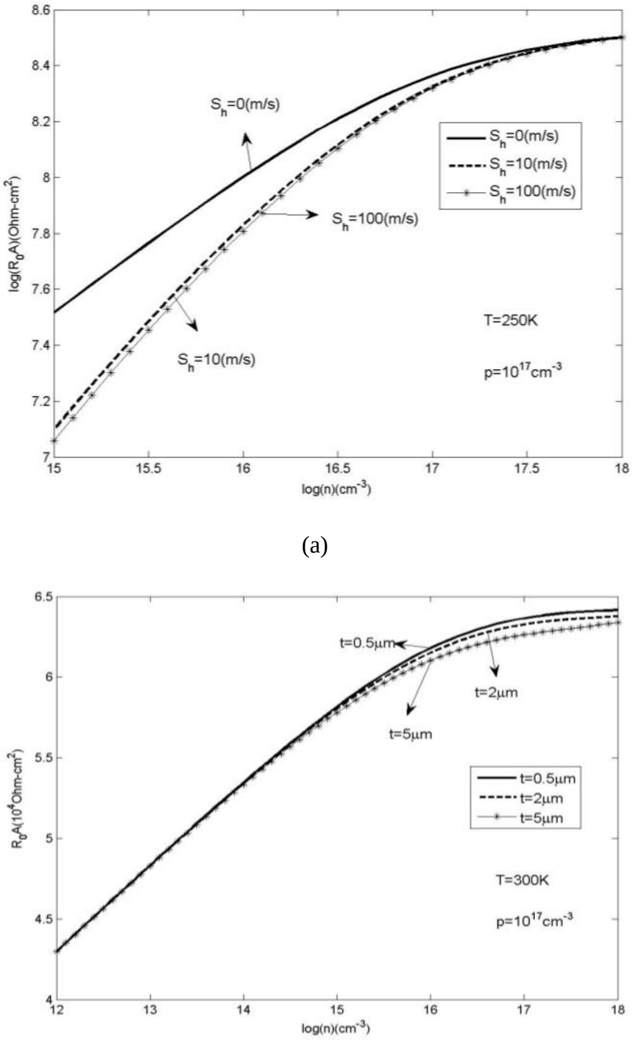

(a)

(b)

Fig. 5. The relationship between n-region carrier concentration on R_0A product with different (a) n-side surface recombination velocity and (b) thickness. t=5μm, d=5μm, S_e=0.

4. Conclusion

Four kinds of noise mechanism have diverse impact on $(R_0A)_{Total}$ at different range of carrier concentration. $(R_0A)_{GR}$ determines $(R_0A)_{Total}$ at low carrier concentration ($p<10^{15}cm^{-3}$). However, when $p>10^{18}cm^{-3}$ and both *p*-region and *n*-region to be degenerate, $(R_0A)_{Total}$ is limited by the Auger mechanism on the triangular barrier and by the Tunneling mechanism on the parabolic barrier. Furthermore, the carrier concentration, thickness and surface recombination velocities in the two quasi-neutral regions have significant influences on R_0A product. The effect of *n*-region parameters on R_0A product is smaller than the *p*-region parameters. It is apparent that the R_0A product increases steadily with increase in *p*-region doping concentration, reaches a peak value and then finally decreases with a further increase in doping concentration. However, R_0A product has been found to increase with *n*-region carrier concentration and tends to be saturated. In addition, the R_0A product of the device is strongly influenced by the operating temperature. The value of R_0A product is $10^8(\Omega{\bullet}cm^2)$ at T=250K while it is $10^6(\Omega{\bullet}cm^2)$ at T=300K. These results will provide a useful guide for designing and fabrication of the $In_{0.53}Ga_{0.47}As$ photovoltaic detectors.

Acknowledgements

This work was supported by Natural Science Foundation of China Contract No. 60676039, 863 Project of China Contract No. 2007AA06Z112, the Science and Technology Department of Jilin Province under Grant No 20070709.

Reference

[1] Yingtian Xu, Ying Li, Beihong Long, Yan Ma, Guotong Du, Jingzhi Yin. Optoelectron. Adv. Mater. - Rapid Comm., **6**(11-12), 1009 (2012).

[2] Xiaofeng Duan, Yongqing Huang, Xiaomin Ren, Yufeng Shang, Xinye Fan, Fuquan Hu. IEEE Photonics Technology Letters. **24**(10), 863 (2012).

[3] Liu Shao-Qing, Han Qin, Zhu Bin, Yang Xiao-Hong, Ni Hai-Qiao, HF Ji-Fang, Wang Xin, Niu Zhi-Chuan. CHIN. PHYS. LETT. **29**(3), 038501 (2012).

[4] Michael MacDougal, Jon Geske, Chad Wang, David Follman. Optical Engineering. **50**(6), 061011 (2011).

[5] A. Tosi, F. Acerbi, A. Dalla Mora, M. A. Itzler, X. Jiang. IEEE Photonics Journal, **3**(1), 31 (2011).

[6] A. Rogalski. Progress in Quantum Electronics, **27,** 59 (2003).

[7] L. Becker. Proc. of SPIE. **5881,** 588105 (2005).

[8] Lars Zimmermann, Joachim John, Stefan Degroote, Gustaaf Borghs, Chris Van Hoof. Appl. Phys. Lett. **82,** 2838 (2003).

[9] V. Gopal, S. K. Singh, R. M. Mehra. Infrared Ph ysics & Technology. **43,** 317 (2002).

[10] P. Chakrabarti, A. Krier, A. F. Morgan. IEEE Transactions on Electron Devices. **50,** 2049 (2003).

[11] P. Chakrabarti, P. K. Saxena, R. K. Lal. International Journal of Infrared and Millimeter Waves. **27,** 1119 (2006).

[12] M. R. Johnson, R. A. Chapman, J. S. Wrobel. Infrared Phys. 15 (1975) 317.

[13] S. M. Sze. Physics of Semiconductor Devices 2nd edn (New York: Wiley) 513, 1981.

[14] Yuchun Chang, Bao Shi, Longhai Li, Jingzhi Yin, Fubin Gao, Guotong Du, Yixin Jin. Solid State Communications. **151,** 1953 (2011).

[15] A. Rogalski, R. Ciupa, Journal of Electronic Materials, **28**, 630 (1999).

[16] Gregory H. Olsen, Marshall J. Cohen, Proc. SPIE. **3379,** 300 (1998).

[17] A. Rogalski. Optoelectronics Review. **5**, 205 (1997).

---

*Corresponding author: yjz886666@163.com